Long-stroke rolling diaphragm actuators for haptic display of forces in teleoperation

Alexander Gruebele[1], Samuel Frishman[1], and Mark R. Cutkosky[1]

***Abstract*—We present a new rolling diaphragm actuator for transmitting forces in a teleoperated system. The initial application is for MR-guided biopsy procedures, providing accurate transmission of motions and forces between the fingertips of a physician and a biopsy needle being inserted into tissue. Desirable actuator qualities include low hysteresis, high axial stiffness, and long travel. The actuator uses an anisotropic laser-patterned fabric embedded in a soft silicone sleeve for a combination of low stretch in the axial direction and sufficient stretch in the radial direction so that a taper is not required; hence the actuator can have almost any length. We present results for a prototype input/output system with 6 cm stroke, 1 cm diameter and a minimum force of 0.3 N to initiate motion. We compare its performance to a system using commercial rolling diaphragm actuators and show that the new system provides an improved combination of long stroke, high stiffness, and accurate transmission of fingertip forces.**

***Index Terms*—Soft Material Robotics, Haptics and Haptic Interfaces, Telerobotics and Teleoperation**

I. Introduction

A. Background

HYDROSTATIC transmissions have a favorable combination of high stiffness, wide force range, and ability to route through complex geometries. As a result, they are used in diversity of applications ranging from car brakes to teleoperated surgical devices [1]. Despite their advantages, traditional hydrostatic systems require dynamic seals which introduce significant friction and the potential for fluid seepage. To overcome these challenges, rolling-diaphragm technologies have been employed in cases where low friction and leak-proof seals are desired. In particular, fiber-reinforced rolling-diaphragms replace dynamic seals (e.g. piston rings) and provide high stiffness with low friction. These properties enable force propagation with little distortion between the input and output of a system. Example applications include human interaction robotics [2], [3], prosthetics [4], [5], and a teleoperated system for remotely operated MR needle insertion [6]. In other applications, they were considered an ideal technology, but could not be used due to their limited stroke [7].

Rolling diaphragm technology has existed since at least the 1920s, with patents dating to 1931 [8]. The manufacturing process used for commercially available fabric-reinforced diaphragms limits the length-to-diameter ratio to approximately one. Suppliers manufacture diaphragms by deep drawing a reinforcing fabric sheet into a mold cavity, injecting an elastomer, and then vulcanizing [9]. The limited deformability of the fabric being drawn bounds the length-to-diameter ratio and furthermore results in a squaring effect [10]. Additionally, due to a centering effect at the ends of the stroke, the usable stroke is further reduced [6]. Alternative manufacturing methods, such as those described in [11] and [4], have been proposed and allow for stroke lengths many times the diaphragm diameter. These methods, however, used a taper that restricts the diameter to length ratio achievable. A weft knit fabric is also suggested in [11] allowing the diaphragm to be cylindrical. However, knit fabrics [12] can produce increased hysteresis which is undesirable in low force applications.

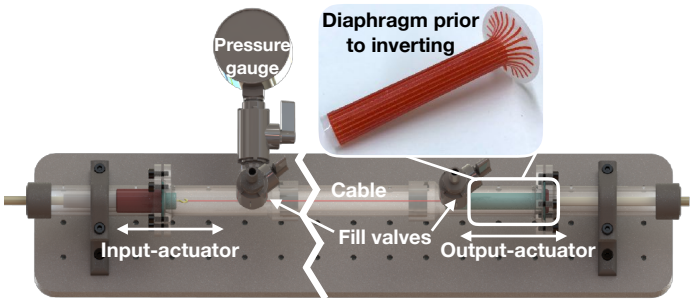

Fig. 1. System of two opposed actuators connected by a Vectran cable to withstand internal pressure. Tube connecting input/output ends can be arbitrarily long. Inset: photo of long-stroke diaphragm before inverting to form convolution.

To overcome the limitations of conventional fabric-reinforced rolling diaphragms we present a novel design and manufacturing method that uses 3D printed molds to create diaphragms with arbitrarily long stroke/diameter ratios. The manufacturing method is described in detail in section II and diaphragm characterization is presented in section V. The new actuator is incorporated into a single-axis input/output system (Fig. 1) which replaces an earlier design described in [6] using commercial short-stroke actuators.

The presented design is an example of selective stiffness in soft robotics [13], specialized for an application where high stiffness is required in one direction along with ease of bending and stretching in an orthogonal direction.

B. Related work

In addition to previously cited developments on rolling diaphragms, the concept of selective compliance has been previously explored and the new design presented draws upon

Manuscript received: September, 10, 2018; Revised December, 4, 2018; Accepted December, 29, 2018

This paper was recommended for publication by Editor Allison M. Okamura upon evaluation of the Associate Editor and Reviewers' comments. This work was supported by NSF CHS 1615891.

[1]Authors are with the Dept. of Mechanical Engineering, Stanford University, Stanford, CA 94305 USA. alexgruebele@stanford.edu

Digital Object Identifier (DOI): see top of this page.

several related technologies. A soft anisotropic pneumatic actuator consisting of paper strips embedded in a sealed elastomeric cylinder was designed such that it contracts axially when inflated, using pressure to achieve linear motion [14]. Since the sidewalls must be unconstrained for motion to take place, this design is compliant. In another actuator, linear motion is achieved by wrapping inextensible fibers around a elastomeric cylinder, mechanically programming the pneumatic actuator's behavior based on fiber angle. When constrained in a tube, successive inflation of the actuators generates locomotion [15]. Fiber reinforcements have also been used to control pneumatic actuator bend radius for grasping. Axial fibers can selectively prevent elastomer extension creating a bend, while circumferentially wrapped fibers prevent pressure bulging and maintain a desired actuator aspect ratio [16].

C. MR-compatible biopsy

With no ferrous components, hydrostatic transmissions are a suitable technology for MRI environments. Previous work [6], [17] has described the challenges associated with limited patient access during image-guided biopsies and the need for an MRI-compatible transmission. Forces experienced during needle insertion are relatively small ($<$ 15 N [18]) and as a result, transmission losses must be low to achieve haptic transparency. Skin-to-target distance varies widely between cases. For liver biopsies, studies report ranges from 22-177 mm [19] and for transperineal prostate biopsy up to 150 mm [20].

II. Design and Fabrication

A. Design

The system illustrated in Fig. 1 has identical actuators at each end. The actuator design is illustrated in Fig. 2. A piston (1) is moved by a rolling diaphragm, which is clamped with a molded-in bead (2) to seal the system. Pressure from the working fluid is primarily distributed along the walls of the bore and piston, leaving the convolution gap (3) as the only unsupported section. The gap allows the piston to translate with virtually no Coulomb friction and the pressure helps center the piston in the bore. As the piston and shaft translate, the diaphragm rolls to expand against the bore wall or contract around the piston (depending on the direction of motion). A shaft (4) provides a connection to the system input or output.

When used in a input/output transmission, diaphragm pairs must be preloaded to balance the pressure. References [3], [5], [21] discuss several preloading solutions. In our experimental setup, we use an internal Vectran cable (5) (TwinLine Braided Vectran 125) attached to opposing piston heads to offset the pressure. This material was chosen for its high stiffness and low creep. The length is set such that when the back of one piston reaches its clamping plane (6), the second piston is furthest back from its clamping plane.

For the diaphragm to remain axially stiff under pressure and external force, the flexible elastomer layer must be supported by a stiff member. In industrial diaphragms, this is typically a woven fabric that is either molded between elastomer layers or bonded to an elastomer surface [10]. To minimize elastomer thickness, and therefore hysteretic losses during motion (discussed in Section III), we design the actuator with one elastomer layer (Fig. 2 item (7)). Furthermore, to reduce elastomer bulging and potential for rupture, we design the actuator with the fabric layer (8) on the dry side of the elastomer. Additionally, we recognize that stiff fibers are only required in the axial direction, so our design has no continuous fibers around the circumference. Rather, it uses 25 individual strips of ripstop nylon cloth with the weave oriented along the axis of the diaphragm for strength (Fig. 1). We chose a room-temperature-vulcanizing (RTV) silicone for ease of molding and due to the low hysteretic losses of silicone rubbers [22], [23].

The actuator prototypes have a length of 60 mm with a piston diameter of 10 mm for a 6:1 length to diameter ratio, as compared to the traditional limit of ≈1:1 for commercial actuators [10]. In the present case, the 6:1 ratio results in a convenient size of fabric for laser patterning. Using the fabrication technique described in II-B, diaphragm length is only limited by manufacturability of the elastomer mold and laser patterning area of the fabric. However, a mold turned from rod stock with machined alignment features could be very long, and a jig could be used to pass a continuous piece of fabric into the laser cut area.

Diaphragm manufacturers recommend that a convolution gap of at least four times the diaphragm thickness is employed [10]. A larger gap reduces system stiffness due to the increased compliance of unsupported elastomer at the convolution. Greater circumferential expansion also results in more hysteric losses due to strain in the elastomer. However, bending stresses in the convolution decrease as the gap increases. We evaluated the minimum force to produce motion for gap sizes from 3 mm to 5.5 mm in 0.5 mm increments, finding the lowest force occurring at a gap size of 5 mm (≈6 times diaphragm thickness) for a 15 mm bore.

B. Fabrication

The core enabling component of the actuator is the rolling diaphragm. The diaphragm consists of a fabric reinforced structure for strength, and a molded silicone sleeve to seal against the fluid. The fabric used is a silicone impregnated ripstop nylon (Silnylon[1]) with a mass of 44 g/m^2 and a

[1]http://www.seattlefabrics.com/

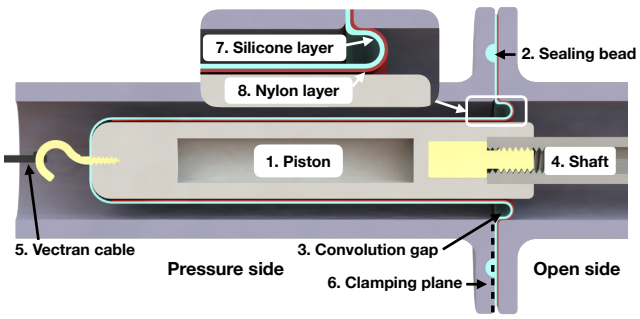

Fig. 2. Cross section of long-stroke actuator installed in bore with Vectran line allowing pressurization without external pre-load. Numbered labels match descriptions in text.

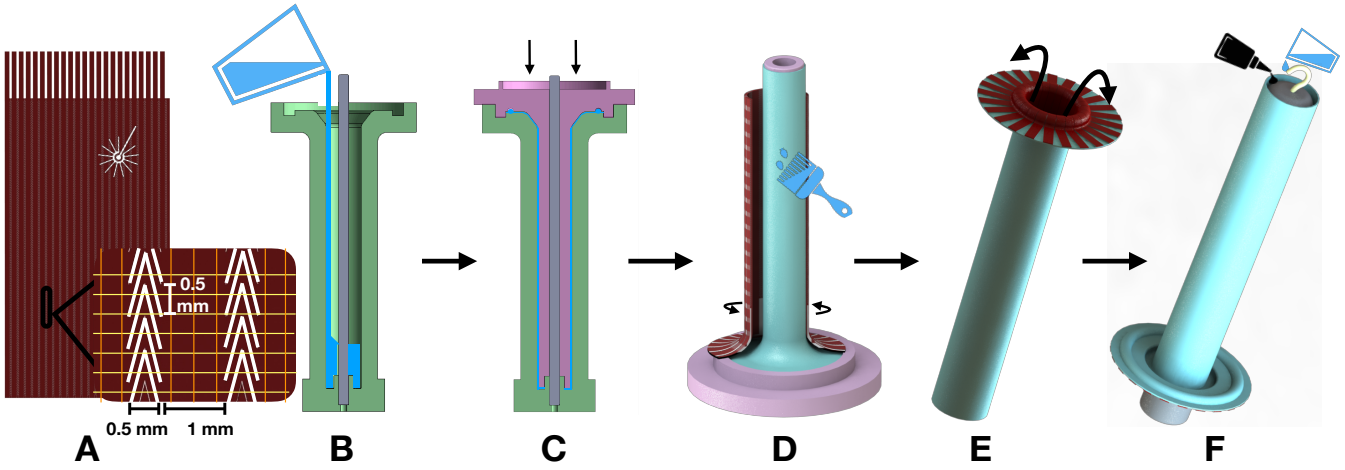

Fig. 3. Fabrication process of long-stroke actuators: (A) Fine chevron pattern laser cut into Silnylon, forming anisotropic fabric (B) Silicone poured into 3D printed mold core (C) Mold assembled and silicone cured (D) de-molded silicone sleeve brushed with thin layer silicone to be tacky, and lasercut mesh adhered to sleeve (E) sleeve inverted so that silicone on exterior when convolution forms (F) fabric glued at the top to the piston and sealed with silicone

thickness 0.07 mm. Although thin, the fabric is relatively inextensible along the primary fibers and its coating promotes adhesion to silicone moldings. A patch of Silnylon is patterned with a diode pumped solid state laser (DPSS[2]) capable of making 15 μm wide cuts. A chevron pattern of V-shaped perforations (Fig. 3 A) results in having no continuous fibers in the circumferential hoop direction, but continuous fibers in the axial direction when wrapped into a cylindrical shape.

Dragonskin 20 room-temperature-cure silicone[3] is mixed with 10% by mass Silicone Thinner to reduce viscosity for molding, and degassed in vacuum. A 3D printed mold cavity (Formlabs[4] Tough photopolymer resin, having similar properties to ABS) and core are sprayed with mold release to aid in finished part removal. The silicone mixture is then poured into the mold cavity and the mold core is pressed into the cavity, forcing excess silicone out of top vents (Fig. 3 B and C). The mold is placed in vacuum to remove any entrapped air and pulled apart after 4 hours of curing. Flash from the vents is trimmed off the finished silicone sleeve (0.30 mm thickness).

With the silicone sleeve on the mold core the sleeve is brushed with a thin layer of Dragonskin 20. Excess is scraped off with a spatula, leaving the surface tacky. The patterned Silnylon mesh is wrapped around the silicone sleeve, such that the strips lay flush against the silicone (Fig. 3 D). At the top, 5 mm of the sleeve is left exposed to allow the diaphragm to be later potted to the piston (Fig. 3 F). Once cured, the diaphragm is inverted, allowing a convolution to form (Fig. 3 E). A 3D printed piston is prepared with a brass hook screwed into the top and a threaded standoff pressed in at the bottom. The hook attaches to the Vectran cable and the threading connects to an external piston rod. In the last step, the diaphragm slides onto the piston and the fabric is glued to the top. The protruding 5mm of sleeve is filled with more Dragonskin 20 to seal the diaphragm around the piston (Fig. 3 F). Upon initial pressurization, the diaphragm will expand to the diameter of the bore. This will tear the sacrificial chevron patterns, leaving many thin vertical strips of fabric to provide axial stiffness.

[2]https://www.dpss-lasers.com
[3]https://www.smooth-on.com
[4]https://formlabs.com

III. Model

When the actuators are integrated into an input/output system, several losses can reduce force transparency. Viscous and choked flow losses can occur especially at joints and tube fittings, hence the diameter of the system should be kept nearly constant throughout. Additionally, fluid mass should be minimized to reduce inertial effects. Viscous drag along the length of the tube cannot be eliminated, but can be minimized by choosing a low viscosity fluid. The Reynold's number is $\mathrm{Re} = \rho \mathrm{Dv}/\mu = 150$ where ρ is the density of water, pipe diameter is $D = 15\,\mathrm{mm}$, μ is the viscosity of water, and $v = 10\,\mathrm{cm/s}$ is the fluid velocity, determined by maximum actuation speed for the intended application. A Reynold's number of 150 is safely in the laminar region, thus the viscous loss depends linearly on velocity of actuation as $F_b = b_{visc}v$.

Figure 4 shows two types of deformation in the diaphragm. The first is the circumferential expansion, ϵ_c, as each cylindrical element of the actuator expands from the piston to the bore, increasing in circumference from $2\pi r_p$ to $2\pi(r_p + t + 2r_c)$, where r_p is piston radius, r_c is convolution radius, and t is actuator thickness. A second deformation arises from bending of the elastomer, ϵ_b, as it makes a 180° turn from piston to bore, with bending radius $r_c + t/2$. Both of these deformations can have a hysteretic component, which is typically not strongly velocity dependent [24], as well as any viscoelastic effects, which can be combined with the viscous losses from the fluid. Both of these terms depend on total elastomer volume in strain; therefore thickness and piston circumference should be minimized to reduce these losses. Moreover, they depend primarily on the geometry of the convolution and not on the applied load, so their effect is most important when applied forces are small. In summary, we can represent the combined minimum force required to actuate the system as $F = C + b_{visc}v$ where C is a constant and $b_{visc}v$ represents velocity dependent terms.

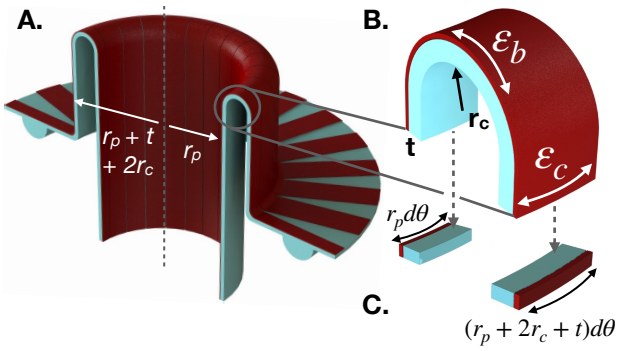

Fig. 4. Two deformations take place as actuator translates. (A) a cutaway of diaphragm showing piston and bore diameters. (B) bending strain occurs as an element rolls across the convolution, (C) circumferential strain occurs as material expands from piston to bore.

At low to moderate frequencies the system can be approximated as a lumped-parameter second-order system:

$$m\ddot{x} + b\dot{x} + kx = F_{in} \tag{1}$$

where b represents the damping terms (elastomer hysteresis, viscous fluid losses), k represents the system stiffness (diaphragm and tubing compliance), m is the mass in motion (fluid, diaphragms, and pistons), and F_{in} is the force at the input. Mass, viscous damping, and stiffness are determined empirically in Section V.

IV. Experiments

Various measures can be used to evaluate performance of a teleoperator [25], depending on the intended application – for example whether the device is manipulated in air, against a stiff environment, or in contact with human tissue. To evaluate the system we conducted several tests. The first measures resistance to motion with output in free air at constant velocity; this test essentially measures friction, viscous, and hysteretic losses in the system. Friction, which is the most problematic for human interaction, is expected to dominate at very low speeds; viscous losses should dominate at higher speeds. The second test measures force tracking for small oscillations of fixed amplitude at various frequencies. The results are affected by mass and damping as accelerations and average speeds increase. The third test measures output/input force as a function of frequency for a sinusoidal input force while the system presses against a spring chosen to approximate the stiffness expected for a human body.

A. Experimental setup

A single degree-of-freedom (DOF) input/output system was constructed to test the performance of the diaphragms. The system was filled with circulating water until all visible air bubbles were removed. A nominal internal pressure of 70 kPa (10 psi) was used for experiments. Brass rods (Fig. 5, item (1)) were screwed into the pistons for input and output connections while the pistons were inside the bores. The rods were supported by low friction nylon swivel bearings (McMaster 1071K12) (Fig. 5, (2)).

For the first experiments, the system was actuated using a linear stage (Fig. 5, (3)) which provided position data with an optical encoder ($< 1\,\mu$m) resolution). A Futek FSH00103 load cell (resolution ≈10.6 mN) (4) was mounted to the linear stage and pushed on the rod connected to the input piston to measure input force. For experiments that also measured output force, an Omega LCFD-5 load cell (resolution ≈10.6 mN) (5) was mounted to the rod at the output end. Both force sensors were sampled by an Arduino Mega with an external 16-bit ADC capable of sampling both sensors at ≈100Hz.

For the constant velocity experiments with the output end in free air, the linear stage moved forward over a 60 mm range at a given velocity while input force was measured. The velocity range was selected based on the upper bound of expected insertion speeds experienced during a needle biopsy procedure.

Input-output force tracking for small motions was evaluated by manipulating the device with the linear stage against a spring (1.26 N/mm, chosen to approximate the stiffness of a human body in an MRI machine) at different frequencies and measuring the input and output forces (Fig. 5, item (6)). The oscillation amplitude was fixed at ≈1 mm, limited by the capabilities of the stage at the higher frequencies. As noted earlier, with fixed amplitude oscillations, speed and acceleration increase with frequency, and the effects of inertia and damping become increasingly important.

Frequency response data were obtained by actuating the system with a 1 N sinusoidal force input using an Aurora Scientific Dual-mode Model 6900 muscle lever against the aforementioned 1.26 N/mm spring. For comparison, the test was repeated using a much stiffer 18 N/mm external spring and a 2 N force amplitude. The stiffer spring, although not realistic for the intended application, was used to clearly separate the resonant response of the entire system, including the environment, from that of the teleoperator itself. An ATI Gamma load cell measured the output force on the external springs, sampled at 1 kHz.

We compared our long-stroke actuators to two other technologies intended for transparent force transmission. We assembled a system of similar dimensions using B. Braun loss-of-resistance (LOR) ground glass syringes[5], filled with a low-viscosity (5cSt) silicone oil[6]. These syringes have traditionally been used for identification of the epidural space by sensing a drop in pressure. They are designed for consistent and smooth motion. Here we fill them with silicone oil instead of water for improved lubricity. Additionally, the silicone oil does not evaporate at room temperature so no fluid is lost as the plunger is exposed. The end of the syringe is cut off in order to remove the constriction and reduce viscous losses. The setup using dual LOR syringes and silicone oil can be considered a "gold standard" for transparent force transmission as they include virtually no Coulombic friction or hysteresis. However, they would be impractical for applications where durability and shock resistance are important. In addition, the syringes are only available in a few standard sizes.

[5]https://www.bbraunusa.com/en/products/b/loss-of-resistancesyringes.html
[6]http://www.clearcoproducts.com/pure-silicone-low-viscosity.html

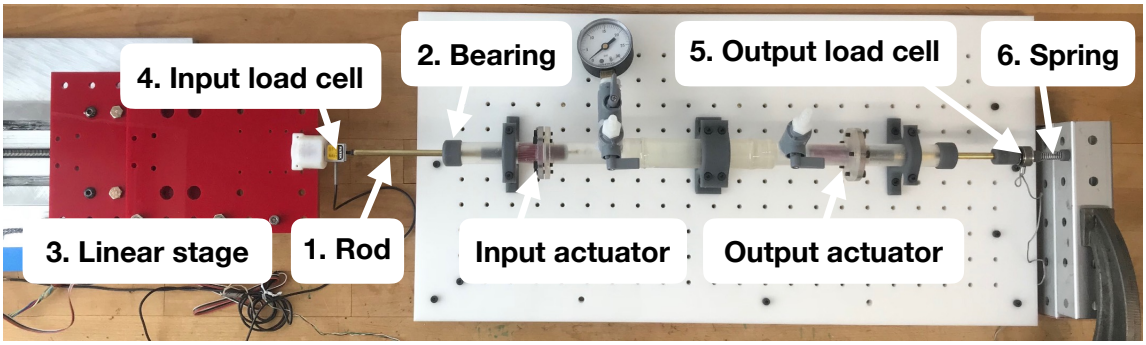

Fig. 5. Experimental setup for measuring force transparency and frequency response of the actuators. The linear stage on the left pushes the input actuator via the input load cell. For frequency response a spring is placed against a hard stop, and output actuator force is measured during oscillation.

We also compared the long-stroke actuators to force-velocity data taken previously using the teleoperator shown in Figs. 1 and 2 of [6]. This system used commercial Fujikura[7] DM4 rolling diaphragms of diameter 20 mm and 20 mm stroke, with displacement amplified through a capstan drive. The data points used are not explicitly presented in [6], however they were obtained from the same data set.

V. Results

A. Force transparency

Figure 6 displays the force required to move the actuators at various velocities when the slave end is in free air. The short-stroke rolling diaphragms had the greatest force-to-move, starting at 0.6 N at ≈7 mm/s. Our long-stroke actuators had a minimum force of 0.27 N, and the LOR ground glass syringes started at 0.06 N. In all cases, the necessary force for motion increases with input velocity linearly due to viscous losses in the tube. The slope is highest for the ground glass syringes due to the use of silicone oil which has a viscosity approximately five times greater than that of water. However the slope of the LOR syringes is not five times greater than that of the long-stroke actuators but rather closer to 1.75 times greater. This is likely because the long-stroke actuators and Fujikura diaphragms have a component of viscoelastic loss that increases proportionally with velocity.

B. Stiffness

The stiffness of the teleoperator system was measured by reading force from the input load cell with the output against a hard stop. Displacements were taken from the linear stage (Fig. 5). The stiffness was found to be 11.74 N/mm and nearly constant ($R^2 = 0.998$ fit) for 2-10 N. The main source of compliance is in the actuators due to bulging of the silicone in the small gaps between the strips of Silnylon fabric support. Additionally, some compliance may occur from any air bubbles trapped in the system and strain in the plastic pipe. The stiffness of the commercial short-stroke diaphragms was not evaluated but is assumed to be substantially higher because they use a dense, continuous sheet of fabric for reinforcement and are designed for higher operating pressures. Shaping the fabric in the commercial manufacturing process is what limits the stroke-to-diameter ratio.

[7]http://www.fujikura.com

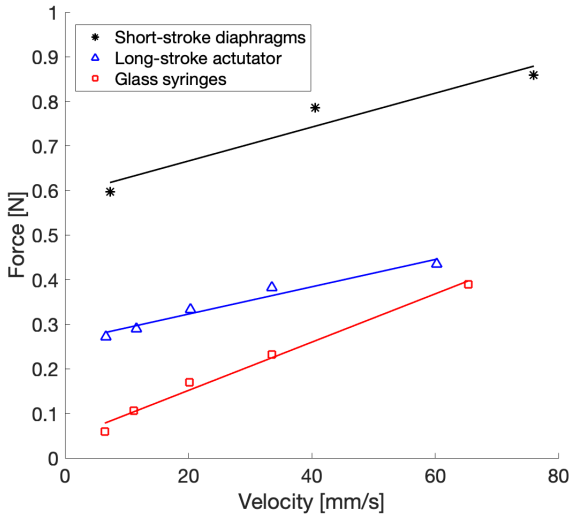

Fig. 6. Forces required to sustain motion at various velocities for a single-axis teleoperation system using: □ seal-less glass syringes with silicone oil, △ new long-stroke rolling diaphragm actuator with water, ∗previous system using commercial short-stroke rolling diaphragms and water [6].

The burst pressure of the long-stroke rolling diaphragms was measured to be 241 kPa. This is much lower than the Fujikura DM4 diaphragms, which are rated to 1.7 MPa. However, for the force ranges relevant to MR-biopsy, such high pressures are not required.

C. Frequency response

Figure 7 shows the difference between input and output force normalized by input force for 1 mm amplitude oscillations at frequencies ranging from 2-9 Hz.

For the glass syringes, higher frequency tends to decrease force transparency, mainly due to viscous losses. The long-stroke actuators show worse force tracking; however, this remains relatively constant with increasing frequency.

The LOR syringes are unaffected by load and show similar performance for both the 1 N and 6.5 N cases. The long-stroke actuators, however, improve in transparency at higher load. This is because the increase in force error at higher loads is proportionally less than the increase in input force. There is also a slight improvement in performance of the long-stroke

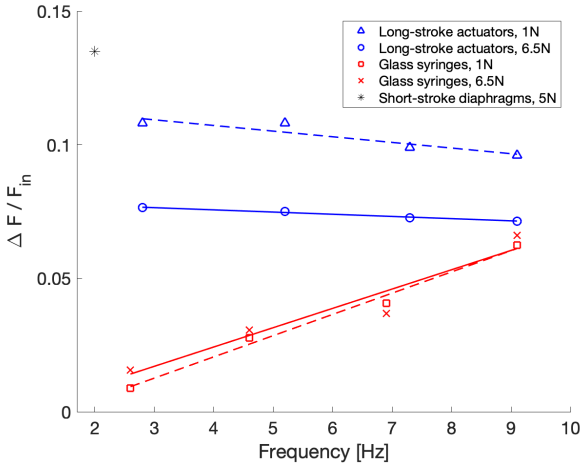

Fig. 7. Force accuracy for glass syringes and long-stroke actuators at 1 N and 6.5 N spring pre-load, and short-stroke rolling diaphragms at 5 N pre-load for 1 mm oscillations at various frequencies.

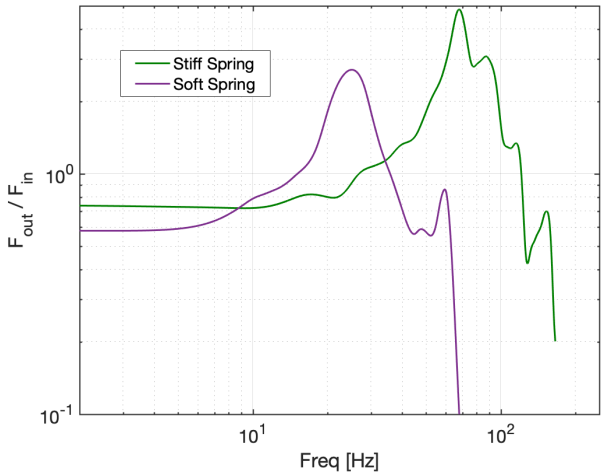

Fig. 8. Frequency response of teleoperator against a soft and a stiff spring.

actuators at higher frequency that is more apparent in the low pre-load case. This may be due to the instantaneous increase in pressure as the mass of fluid is accelerated during each cycle (which has greater relative impact when it starts at a lower pressure at 1 N pre-load). As the cycles become shorter with increasing frequency, this increase in pressure becomes more important, aiding the rolling motion of the convolution. In all cases, the actuators come in at less than 11% force loss relative to input. This is better than the commercial short-stroke diaphragm which has ≈ 13.5% force loss at 2Hz (single point data from [6]).

Figure 8 illustrates response of the system for frequencies from 2 to over 100 Hz (well above the expected frequency range for the system). When manipulated against the 1.26 N/mm spring, the response is dominated by resonance of the entire system with the soft external spring. The peak at 25 Hz approximately matches the calculated frequency given the measured mass and damping: (m = 0.09 kg, b = 0.003 Ns/mm). A second peak is seen at ≈60Hz and corresponds to the resonance of the teleoperator given its stiffness (11.74 N/mm). In the stiff external spring test (k_e = 18 N/mm) the overall system resonance shifts to ≈66Hz, at which frequency the teleoperator system can no longer be approximated as a single mass. However, the output/input force tracks well until ≈25 Hz. Below 10 Hz hysteretic and viscous effects keep the output force somewhat below the input force, consistent with data in Fig 6.

VI. Discussion

The long-stroke actuators result in a responsive system with improved force transparency over commercially available fabric reinforced diaphragms in the 1-15 N force range. This is expected as commercial diaphragms are typically manufactured for high pressure applications with limited consideration for hysteresis and other losses (e.g squaring and centering effects). The long-stroke actuators exhibit more compliance than commercial diaphragms because they have small gaps between the reinforcing strips, resulting in some bulging of the elastomer. This can be improved with an increase in slit number and a decrease in the convolution gap radius. Even so, the current implementation provides adequate stiffness for many low and medium force applications including MRI-guided needle biopsy.

Measuring frequency response of the teleoperator against a soft spring (Figure 8), we are able to validate a second-order lumped-parameter model for forces and velocities of practical interest. The system has a nearly constant output/input force ratio for frequencies up to 25 Hz, which is generally considered to be more than adequate for human-initiated motions [25]. However, humans can sense force transients and vibrations at much higher frequencies than they can control. Thus future work could include adding vibrational or skin-stretch cutaneous haptic display (e.g., [26]–[28]) for frequencies that exceed the bandwidth of the teleoperator.

Among the desirable properties for a mechanical teleloperator are low mass, high stiffness and low to moderate damping. Coulomb friction and backlash are undesirable as they impart a highly nonlinear behavior. The system presented here has essentially no backlash because there are no clearances or other sources of lost motion in the system. With no sliding seals, Coulomb friction is also very low. However, there is some resistance to motion due to hysteresis and viscous drag. These effects do not significantly mask forces experienced during biopsy procedures, which can be as large as 15 N [18]. There is additionally a slight centering force at the ends of stroke as the convolution reaches the molded ends of its travel. The solution is to make the diaphragm with a travel slightly longer than the minimum necessary for the application.

The distance from inside the MR-bore to the operator standing outside can be a few meters. Over these distances, care must be taken to limit system compliance, using rigid tubing or reinforced hose. Additionally, viscous losses increase with length, however at the relevant velocities they remain very low if tube diameter is kept constant. At the relevant actuation speeds and current tube diameter (15 mm) a 10 m length of tube would amount to 14 Pa of loss, which is negligible relative to the operating pressure of 69 kPa.

The teleoperator described uses straight, rigid tubing. However, for MRI applications and, particularly, liver biopsy,

tubing may need to bend to orient the needle correctly with respect to the patient. The string-based method to pre-load the system is feasible in this case; however, routing becomes challenging for complex geometries. Methods with internal bearings at 90 degree joints have been successfully prototyped with little increased friction. These designs used rigid tubing; other methods would be necessary for flexible tubing. One potential solution is to use internal low-friction (e.g. Teflon) beads that guide the cable. An alternative pre-loading approach, described in [3] uses a pressurized pneumatic line for pre-loading the system. Non-ferrous versions of all components necessary have been identified to make the system MR-compatible.

VII. Conclusions

We have presented a new design and manufacturing process for long-stroke fiber-reinforced rolling diaphragms. In comparison to many soft-robotic actuators, the diaphragms provide high stiffness and low hysteresis, making them suitable for haptic and teleoperator applications with fingertip force levels. Additional improvements to the manufacturing process will permit the fabrication of actuators with higher stiffness and longer stroke, which should increase the range of operating forces and frequencies they are subjected to. With a higher percentage of reinforcing fibers, the actuators will also become more durable and able to work with higher fluid pressures.

Experiments with an input/output teleoperator using the actuators demonstrate improved performance over previous systems that amplify the motion of commercial rolling diaphragms. Future work includes using higher working pressures, testing additional working fluids with low viscosity and high lubricity such as the silicone oil used with the glass syringes in comparison tests, and expansion to multiple DOF systems.

Acknowledgment

This work is supported by NSF CHS 1615891. A. Gruebele is supported by a Stanford Graduate Fellowship. We thank Dr. B. Gillespie for suggesting LOR syringes as a comparison and we thank our collaborator, Dr. J. P. Whitney, for his insights on hydrostatic transmissions with rolling-diaphragm actuators.

References

[1] R. Gassert, R. Moser, E. Burdet, and H. Bleuler, "Mri/fmri-compatible robotic system with force feedback for interaction with human motion," vol. 11, pp. 216–224, IEEE, 2006.

[2] S. Buerger, "Stable, high-force, low-impedance robotic actuators for human-interactive machines," in *PhD Thesis*, 2005.

[3] J. P. Whitney, M. F. Glisson, E. L. Brockmeyer, and J. K. Hodgins, "A low-friction passive fluid transmission and fluid-tendon soft actuator," in *Intelligent Robots and Systems (IROS)*, pp. 2801–2808, IEEE, 2014.

[4] S. Hashemi and W. K. Durfee, "Low friction, long-stroke rolling diaphragm cylinder for passive hydraulic rehabilitation robots," in *Design of Medical Devices Conference*, ASME, 2017.

[5] Z. Gan, K. Fry, R. B. Gillespie, and C. D. Remy, "A novel variable transmission with digital hydraulics," in *Intelligent Robots and Systems (IROS), 2015 IEEE/RSJ International Conference on*, pp. 5838–5843, IEEE, 2015.

[6] N. Burkhard, S. Frishman, A. Gruebele, J. P. Whitney, R. Goldman, B. Daniel, and M. Cutkosky, "A rolling-diaphragm hydrostatic transmission for remote mr-guided needle insertion," in *Robotics and Automation (ICRA)*, pp. 1148–1153, IEEE, 2017.

[7] G. Pfreundschuh, V. Kumar, and T. Sugar, "Design and control of a 3 dof in-parallel actuated manipulator," in *Proceedings - IEEE International Conference on Robotics and Automation*, vol. 2, pp. 1659–1664, Publ by IEEE, 1991.

[8] C. Farmer, "Flexible diaphragm," in *US Patent 1,790,206*, 1931.

[9] C. Gibson, "Injection molding of fabric reinforced elastomeric diaphragms," in *US Patent 5,093,067*, 1992.

[10] Simrit, "Simrit diaphragm design manual," 2009.

[11] D. Turner, "Tubular rolling diaphragms," in *US Patent 3,403,603*, 1992.

[12] M.-S. Choi and S. P. Ashdown, "Effect of changes in knit structure and density on the mechanical and hand properties of weft-knitted fabrics for outerwear," *Textile Research Journal*, vol. 70, no. 12, pp. 1033–1045, 2000.

[13] M. Manti, V. Cacucciolo, and M. Cianchetti, "Stiffening in soft robotics: a review of the state of the art," *IEEE Robotics & Automation Magazine*, vol. 23, no. 3, pp. 93–106, 2016.

[14] R. V. Martinez, C. R. Fish, X. Chen, and G. M. Whitesides, "Elastomeric origami: programmable paper-elastomer composites as pneumatic actuators," *Advanced functional materials*, vol. 22, no. 7, pp. 1376–1384, 2012.

[15] F. Connolly, P. Polygerinos, C. J. Walsh, and K. Bertoldi, "Mechanical programming of soft actuators by varying fiber angle," *Soft Robotics*, vol. 2, no. 1, pp. 26–32, 2015.

[16] K. C. Galloway, P. Polygerinos, C. J. Walsh, and R. J. Wood, "Mechanically programmable bend radius for fiber-reinforced soft actuators," in *Advanced Robotics (ICAR), 2013 16th International Conference on*, pp. 1–6, IEEE, 2013.

[17] S. Elayaperumal, M. R. Cutkosky, P. Renaud, and B. L. Daniel, "A passive parallel master–slave mechanism for magnetic resonance imaging-guided interventions," *Journal of medical devices*, vol. 9, no. 1, p. 011008, 2015.

[18] T. Podder, D. Clark, J. Sherman, D. Fuller, E. Messing, D. Rubens, J. Strang, R. Brasacchio, L. Liao, W.-S. Ng, *et al.*, "In vivo motion and force measurement of surgical needle intervention during prostate brachytherapy," *Medical physics*, vol. 33, no. 8, pp. 2915–2922, 2006.

[19] M. Moche, S. Heinig, N. Garnov, J. Fuchs, T.-O. Petersen, D. Seider, P. Brandmaier, T. Kahn, and H. Busse, "Navigated mri-guided liver biopsies in a closed-bore scanner: experience in 52 patients," *European radiology*, vol. 26, no. 8, pp. 2462–2470, 2016.

[20] G. S. Fischer, I. Iordachita, C. Csoma, J. Tokuda, S. P. DiMaio, C. M. Tempany, N. Hata, and G. Fichtinger, "Mri-compatible pneumatic robot for transperineal prostate needle placement," *IEEE/ASME transactions on mechatronics*, vol. 13, no. 3, pp. 295–305, 2008.

[21] S. Hashemi, S. Sobojinski, and W. K. Durfee, "Low-friction antagonist hydraulic transmission using long-stroke rolling diaphragm cylinders," in *ASME/BATH 2017 Symposium on Fluid Power and Motion Control*, pp. V001T01A073–V001T01A073, American Society of Mechanical Engineers, 2017.

[22] S. O'sullivan, R. Nagle, J. McEwen, and V. Casey, "Elastomer rubbers as deflection elements in pressure sensors: investigation of properties using a custom designed programmable elastomer test rig," *Journal of Physics D: Applied Physics*, vol. 36, no. 15, p. 1910, 2003.

[23] J. C. Lötters, W. Olthuis, P. Veltink, and P. Bergveld, "The mechanical properties of the rubber elastic polymer polydimethylsiloxane for sensor applications," *Journal of micromechanics and microengineering*, vol. 7, no. 3, p. 145, 1997.

[24] S. Reese, "Meso-macro modelling of fibre-reinforced rubber-like composites exhibiting large elastoplastic deformation," *International Journal of Solids and Structures*, vol. 40, no. 4, pp. 951–980, 2003.

[25] T. L. Brooks, "Telerobotic response requirements," in *Systems, Man and Cybernetics, 1990. Conference Proceedings., IEEE International Conference on*, pp. 113–120, IEEE, 1990.

[26] D. A. Kontarinis and R. D. Howe, "Tactile display of vibratory information in teleoperation and virtual environments," *Presence: Teleoperators & Virtual Environments*, vol. 4, no. 4, pp. 387–402, 1995.

[27] W. McMahan, J. M. Romano, A. M. A. Rahuman, and K. J. Kuchenbecker, "High frequency acceleration feedback significantly increases the realism of haptically rendered textured surfaces," in *Haptics Symposium, 2010 IEEE*, pp. 141–148, IEEE, 2010.

[28] A. K. Han, J. H. Bae, K. C. Gregoriou, C. J. Ploch, R. E. Goldman, G. H. Glover, B. L. Daniel, and M. R. Cutkosky, "Mr-compatible haptic display of membrane puncture in robot-assisted needle procedures," *IEEE Transactions on Haptics*, 2018.